Gated STED microscopy with time-gated single-photon avalanche diode

Iván Coto Hernández,[1,2,6] **Mauro Buttafava,**[3,6] **Gianluca Boso,**[3,4] **Alberto Diaspro,**[1,2,5] **Alberto Tosi,**[3] **and Giuseppe Vicidomini**[1,*]

[1]*Nanoscopy, Nanophysics, Istituto Italiano di Tecnologia, Via Morego 30, 16163, Genoa, Italy*
[2]*Department of Physics, University of Genoa, Via Dodecaneso 33, 16146, Genoa, Italy*
[3]*Dipartimento di Elettronica, Informazione e Bioingegneria, Politecnico di Milano, Piazza Leonardo Da Vinci 32, 20133, Milan, Italy*
[4]*Group of Applied Physics, University of Geneva, Chemin de Pinchat 22, 1211, Geneva 4, Switzerland*
[5]*Nikon Imaging Center, Via Morego 30, 16163, Genoa, Italy*
[6]*These authors contributed equally*
[*]*giuseppe.vicidomini@iit.it*

Abstract: Stimulated emission depletion (STED) microscopy provides fluorescence imaging with sub-diffraction resolution. Experimentally demonstrated at the end of the 90s, STED microscopy has gained substantial momentum and impact only in the last few years. Indeed, advances in many fields improved its compatibility with everyday biological research. Among them, a fundamental step was represented by the introduction in a STED architecture of the time-gated detection, which greatly reduced the complexity of the implementation and the illumination intensity needed. However, the benefits of the time-gated detection came along with a reduction of the fluorescence signal forming the STED microscopy images. The maximization of the useful (within the time gate) photon flux is then an important aspect to obtain super-resolved images. Here we show that by using a fast-gated single-photon avalanche diode (SPAD), i.e. a detector able to rapidly (hundreds picoseconds) switch-on and -off can improve significantly the signal-to-noise ratio (SNR) of the gated STED image. In addition to an enhancement of the image SNR, the use of the fast-gated SPAD reduces also the system complexity. We demonstrate these abilities both on calibration and biological sample. The experiments were carried on a gated STED microscope based on a STED beam operating in continuous-wave (CW), although the fast-gated SPAD is fully compatible with gated STED implementations based on pulsed STED beams.

OCIS codes: (170.6920) Time-resolved imaging; (180.0180) Microscopy; (180.2520) Fluorescence Microscopy; (230.5160) Photodetectors

References and links

1. S. W. Hell, "Microscopy and its focal switch," Nat. Methods **6**, 24–32 (2009).
2. S. W. Hell and J. Wichmann, "Breaking the diffraction resolution limit by stimulated emission: stimulated-emission-depletion fluorescence microscopy," Opt. Lett. **19**, 780–782 (1994).
3. T. A. Klar and S. W. Hell, "Subdiffraction resolution in far-field fluorescence microscopy," Opt. Lett. **24**, 954–956 (1999).
4. H. Blom and J. Widengren, "STED microscopy - towards broadened use and scope of applications," Curr. Opin. Chem. Biol. **20**, 127–133 (2014).

5. D. Wildanger, E. Rittweger, L. Kastrup, and S. W. Hell, "STED microscopy with a supercontinuum laser source," Opt. Express **16**, 9614–9621 (2008).
6. B. R. Rankin, R. R. Kellner, and S. W. Hell, "Stimulated-emission-depletion microscopy with a multicolor stimulated-raman-scattering light source," Opt. Lett. **33**, 2491–2493 (2008).
7. J. Bückers, D. Wildanger, G. Vicidomini, L. Kastrup, and S. W. Hell, "Simultaneous multi-lifetime multi-color sted imaging for colocalization analyses," Opt. Express **19**, 3130–3143 (2011).
8. S. Schrof, T. Staudt, E. Rittweger, N. Wittenmayer, T. Dresbach, J. Engelhardt, and S. W. Hell, "STED nanoscopy with mass-produced laser diodes," Opt. Express **19**, 8066–8072 (2011).
9. V. Mueller, C. Eggeling, C. Karsol, and D. von Gegerfelt, "CW DPSS laser make STED microscopy more practical," Biophotonics **19**, 30–32 (2012).
10. I. Coto Hernàndez, M. d'Amora, A. Diaspro, and G. Vicidomini, "Influence of laser intensity noise on gated CW-STED microscopy," Laser Phys. Lett. **11**, 095603 (2014).
11. B. Hein, K. I. Willig, C. A. Wurm, V. Westphal, S. Jakobs, and S. W. Hell, "Stimulated emission depletion nanoscopy of living cells using SNAP-tag fusion proteins," Biophys. J. **98**, 158–163 (2010).
12. W. I. Zhang, H. Rhse, S. O. Rizzoli, and F. Opazo, "Fluorescent in situ hybridization of synaptic proteins imaged with super-resolution sted microscopy," Microsc. Res. Tech. pp. n/a–n/a (2014).
13. G. Lukinavicius, L. Reymond, E. D'Este, A. Masharina, F. Gottfert, H. Ta, A. Guther, M. Fournier, S. Rizzo, H. Waldmann, C. Blaukopf, C. Sommer, D. W. Gerlich, H.-D. Arndt, S. W. Hell, and K. Johnsson, "Fluorogenic probes for live-cell imaging of the cytoskeleton," Nat Meth **11**, 731–733 (2014).
14. K. Kolmakov, C. A. Wurm, D. N. H. Meineke, F. Gttfert, V. P. Boyarskiy, V. N. Belov, and S. W. Hell, "Polar red-emitting rhodamine dyes with reactive groups: Synthesis, photophysical properties, and two-color STED nanoscopy applications," Chem. Eur. J. **20**, 146–157 (2014).
15. R. Zanella, G. Zanghirati, R. Cavicchioli, L. Zanni, P. Boccacci, M. Bertero, and G. Vicidomini, "Towards real-time image deconvolution: application to confocal and STED microscopy," Sci. Rep. **3**, 2523 (2013).
16. M. Castello, A. Diaspro, and G. Vicidomini, "Multi-images deconvolution improves signal-to-noise ratio on gated stimulated emission depletion microscopy," Appl. Phys. Lett. **105**, 234106 (2014).
17. E. Auksorius, B. R. Boruah, C. Dunsby, P. M. P. Lanigan, G. Kennedy, M. A. A. Neil, and P. M. W. French, "Stimulated emission depletion microscopy with a supercontinuum source and fluorescence lifetime imaging," Opt. Lett. **33**, 113–115 (2008).
18. J. R. Moffitt, C. Osseforth, and J. Michaelis, "Time-gating improves the spatial resolution of STED microscopy," Opt. Express **19**, 4242–4254 (2011).
19. G. Vicidomini, G. Moneron, K. Y. Han, V. Westphal, H. Ta, M. Reuss, J. Engelhardt, C. Eggeling, and S. W. Hell, "Sharper low-power STED nanoscopy by time gating," Nat. Methods **8**, 571–573 (2011).
20. G. Vicidomini, A. Schönle, H. Ta, K. Y. Han, G. Moneron, C. Eggeling, and S. W. Hell, "STED nanoscopy with time-gated detection: Theoretical and experimental aspects," PLoS ONE **8**, e54421 (2013).
21. F. Gottfert, C. A. Wurm, V. Mueller, S. Berning, V. C. Cordes, A. Honigmann, and S. W. Hell, "Coaligned dual-channel sted nanoscopy and molecular diffusion analysis at 20 nm resolution," Biophys. J. **105**, L01 – L03 (2013).
22. G. Donnert, J. Keller, R. Medda, M. A. Andrei, S. O. Rizzoli, R. Lhrmann, R. Jahn, C. Eggeling, and S. W. Hell, "Macromolecular-scale resolution in biological fluorescence microscopy," Proc. Natl. Acad. Sci. U. S. A. **103**, 11440–11445 (2006).
23. G. Vicidomini, G. Moneron, C. Eggeling, E. Rittweger, and S. W. Hell, "STED with wavelengths closer to the emission maximum," Opt. Express **20**, 5225–5236 (2012).
24. E. Ronzitti, B. Harke, and A. Diaspro, "Frequency dependent detection in a STED microscope using modulated excitation light," Opt. Express **21**, 210–219 (2013).
25. I. Coto Hernàndez, C. Peres, F. Cella Zanacchi, M. d'Amora, S. Christodoulou, P. Bianchini, A. Diaspro, and G. Vicidomini, "A new filtering technique for removing anti-Stokes emission background in gated CW-STED microscopy," J. Biophotonics **7**, 376–380 (2014).
26. A. Tosi, A. D. Mora, F. Zappa, A. Gulinatti, D. Contini, A. Pifferi, L. Spinelli, A. Torricelli, and R. Cubeddu, "Fast-gated single-photon counting technique widens dynamic range and speeds up acquisition time in time-resolved measurements," Opt. Express **19**, 10735–10746 (2011).
27. M. Buttafava, G. Boso, A. Ruggeri, A. Dalla Mora, and A. Tosi, "Time-gated single-photon detection module with 110 ps transition time and up to 80 MHz repetition rate," Rev. Sci. Instrum. **85**, 083114 (2014).
28. S. Galiani, B. Harke, G. Vicidomini, G. Lignani, F. Benfenati, A. Diaspro, and P. Bianchini, "Strategies to maximize the performance of a STED microscope," Opt. Express **20**, 7362–7374 (2012).
29. Y. Wang, C. Kuang, Z. Gu, Y. Xu, S. Li, X. Hao, and X. Liu, "Time-gated stimulated emission depletion nanoscopy," Opt. Eng. **52**, 093107–093107 (2013).
30. G. Vicidomini, I. Coto Hernàndez, M. d'Amora, F. Cella Zanacchi, P. Bianchini, and A. Diaspro, "Gated CW-STED microscopy: A versatile tool for biological nanometer scale investigation," Methods **66**, 124–130 (2014).
31. X. Wu, L. Toro, E. Stefani, and Y. Wu, "Ultrafast photon counting applied to resonant scanning STED microscopy," J. Microsc. **257**, 31–38 (2015).

1. Introduction

At the turn of this century, new far-field fluorescence microscopy approaches, usually referred as super-resolved fluorescence microscopy techniques, had effectively overcome the spatial resolution limit imposed by the diffraction phenomena [1]. Similar to conventional fluorescence microscopy, these super-resolved techniques give non-destructive access to the interior of living cells and to the sub-surface of tissues and provide excellent molecular specificity and sensitivity. In addition, they can discern sub-cellular features with sub-diffraction size ($\leq$ 200 nm), which are precluded to conventional fluorescence microscopy.

Theoretically proposed in 1994 [2], and experimentally validated in 1999 [3], stimulated emission depletion (STED) microscopy was the first effective super-resolved microscopy technique [4]. In a STED microscope the diffraction limit is overcome by reducing the size of the effective fluorescence volume of a scanning microscope, which, in a conventional microscope, corresponds to the diffraction limited focus of the excitation laser beam. To this end, the excitation beam of a conventional scanning microscope is overlaid by a second beam, the so called STED beam, whose wavelength is tuned to induce stimulated emission (SE) on the excited fluorophores and whose shape is structured like a doughnut with a "zero"-intensity point into the centre. If the intensity of the STED beam is strong enough, the SE process transiently quenches fluorophores into the periphery of the excitation focus and only the fluorophores in a tiny sub-diffraction region in proximity of the doughnut centre can fluoresce.

Supported by strong developments and progresses in many fields, like laser technology [5–10], labelling protocols [11–14], image analysis/process [15, 16] and photosensitive devices, the STED microscope has become in the last few years a mature technique able to contribute to the solution of many puzzling mysteries in life sciences. An important milestone in the dissemination of STED microscopy was the introduction of the time-gated STED implementation [17–20]. Collecting the fluorescence signal only after a certain time T_g from the fluorophore's excitation event ($t = 0$) and providing that during this time ($0 \leq t \leq T_g$) the fluorophore is subjected to the stimulating photons, the time-gating reduces substantially the STED beam intensity needed to silence the fluorophore. Indeed, the efficiency of signal depletion, i.e. the probability to silence a fluorophore by stimulated emission, depends on the number of stimulating photons to which the fluorophore is exposed while residing in the excited-state. Thus, the time-gated detection ensures that the signal collected stems only from fluorophores that have resided into the excited-state for at least a time T_g and thereby has been exposed to the STED beam at least for the same time.

The reduction of STED beam intensity obtained thanks to the time-gating detection leads to a double improvement. First, photodamage effects are reduced, since they scale in most of the case supra-linearly with the light intensity. Second, the complexity and cost to implement a STED microscope are reduced, since the the STED beam can be implemented using nanoseconds pulsed lasers [21] and eventually continuous-wave (CW) lasers [19], instead of mode-locked femtoseconds/picoseconds pulsed lasers [3, 22]. In particular, when the time-gated detection is combined with a STED beam running in CW, i.e., the so called gated CW-STED (gCW-STED) implementation [19], it is possible to obtain a cheap, easy to implement and low intensity STED microscope. Furthermore, in the gCW-STED microscope, since the STED beam acts continuously during all the time-course of the measurement, the spatial resolution of the system can be "infinitely" increased, at least theoretically, by increasing the time-delay T_g of the detection. Conversely, in a time-gated STED implementation based on a pulsed STED the resolution improvement is obtained only for time-delay T_g up to the pulse width T_{STED} [20] of the STED beam.

The major drawback of the time-gated STED implementations is the reduction of the signal-to-noise/background ratio (SNR and SBR) which is intrinsic to a time-gated detection [20].

Indeed, the fluorescence signal F collected from the center of the doughnut scales exponentially with the time-delay T_g, i.e., $F \sim \exp(-T_g/\tau)$, where τ is the excited-state lifetime of the fluorophore (in absence of stimulating photons). Thus, it is clear that any strategy to reduce the noise/background and to maximize the signal in a gated STED experiment can be very important. Within this scenario, gated STED microscopy has been combined with lock-in (or synchronous) detection architectures to remove the anti-Stokes fluorescent background potentially generated by the STED beam [23–25] and with image processing to improve the SNR [15, 16].

In this study we report about an efficient time-gated implementation able to substantially improve the signal of a gated STED microscope, thus compensating for SNR and SBR reduction. In particular we show that the useful (after T_g) photon flux recorded by the detector in a gated STED microscopy experiment can be increased by implementing a real-time gated detection with a fast-gated single photon detector [26,27], namely a detector that can be switched ON and OFF with few hundreds picoseconds transition time. Up to now, gated STED has been implemented by using time-correlated single-photon counting (TCSPC) cards [17, 19, 20, 23, 28–30] or special gated-boxes [19, 21, 23, 31]. In both cases the photons are registered independently on their arrival times, and sorted in post-processing. This means that also the early-emitted photons (before T_g) are registered, nevertheless, they are later discarded. Thus, the effective maximum count rate of the detection system is reduced. This is due to the so called "pile-up" effect: both the single-photon detector and the TCSPC system have dead-times in the order of tens of nanoseconds that mask late photons arriving few nanoseconds after early photons (i.e. during the dead-time). In a gated STED experiment, this problem prevents to acquire a useful late-emitted photon when a useless early-emitted one has been detected in the same excitation cycle.

We demonstrate the use of a fast-gated detector in a gCW-STED microscopy implementation, however the same results are valid also for gated-STED implementations based on pulsed STED beams.

2. Methods

2.1. CW-STED Microscope

Our CW-STED microscope setup [25, 30] (Fig. 1) featured a 577 nm, continuous-wave (CW) optical pumped semiconductor laser (OPSL, Genesis CX STM-2000, Coherent) for stimulated emission [10] and a home-made super-continuum source for excitation. We generated the super-continuum source by pumping a photonic crystal fibre (femtoWHITE-800, NKT Photonics) with a femtosecond mode-locked Ti:Sapphire laser with a 80 MHz repetition rate (Chamaleon, Vision II, Coherent). Before injection into the CW-STED microscope, the super-continuum beam was temporally stretched ($\sim$ 50 ps) with a 20 m long polarization maintaining fibre (PM460HP, Thorlabs) and spectrally filtered (488 $\pm$ 3 nm) with a laser clean-up filter (Bright Line HC 488/6 nm, AHF Analysentechnik) to obtain the blue picosecond pulsed excitation beam for the experiments. We generated the doughnut-like intensity distribution of the STED beam by introducing in the STED beam path a polymeric mask imprinting $0-2\pi$ helical phase-ramp (VPP-A1, RPC Photonics), that we imaged into the back aperture of a 1.4 NA objective lens (HCX PL APO, 100$\times$ 1.40, oil, Leica). We aligned the excitation and STED beams on the same optical axis by using custom-made dichroic mirrors (AHF Analysentechnik). We used two fast-moving galvanometric silver-mirrors (6215HM40B, CTI-Cambridge) to scan the two co-aligned beams over the sample. We collected the fluorescence through the same objective lens, we de-scanned it, we filtered it out with an appropriate bandpass filter (ET Bandpass 525/50 nm, AHF Analysentechnick) and we imaged it with a 60 mm doublet lens (AC254-060-A-ML, Thorlabs) into the active area of the fast-gated detector. Importantly, the 50 μm diameter of

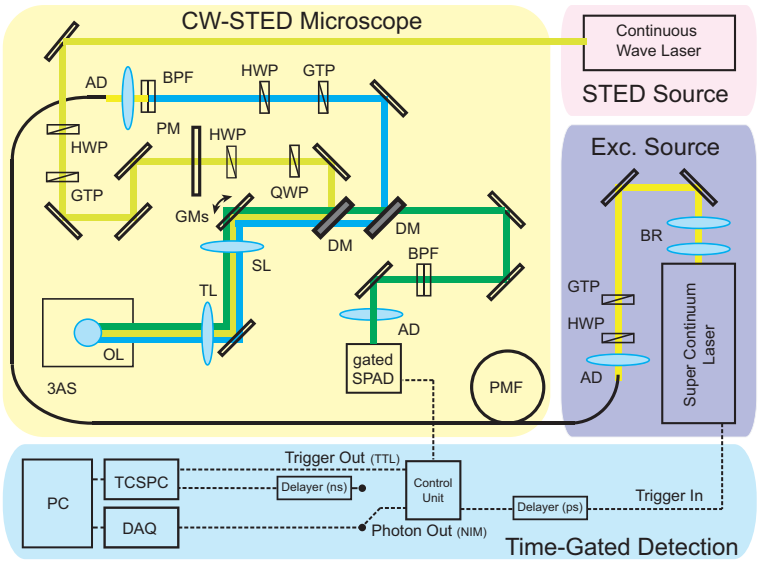

Fig. 1. Experimental gCW-STED setup integrated with the fast-gated SPAD module. HWP: half-wave plate; QWP: quarter-wave plate; GTP: Glam–Thompson polarizer; PM: phase mask; DM: dichroic mirror; GMs: galvanometer mirrors; SL: scanning lens; TL: tube lens; OL: objective lens; 3AS: three-axis stage; BPF: band-pass filter; PMF: polarization-maintaining fibre; SPAD: single-photon avalanche diode; AD: achromatic doublet; BR: beam reducer; PC: personal computer; TCSPC: time-correlated single photon counting; DAQ: data acquisition.

the SPAD area is about an Airy disc of the imaged excitation point-spread-function (PSF). We used the software Imspector (Imspector, Max Planck Innovation) to manage all the acquisition operations. We measured all power values for the excitation and STED beams at the back aperture of the objective lens. The average STED intensity at the doughnut crest is estimated by $I^m_{STED} = kP_{STED}/A_{STED}$, where A_{STED} denotes the STED focal area of the diffraction limited Gaussian spot and $k = 0.3$ is a scaling factor which takes into account the larger area of the doughnut. We determined $A_{STED} \sim \pi(FWHM_{STED}/2)^2$ from the full-width at half-maximum ($FWHM_{STED}$) of the diffraction limited Gaussian spot. The value of $FWHM_{STED} \sim 270$ nm was measured by imaging a sub-diffraction sized gold bead (80 nm gold colloid, EmGC80, BBinternational, Cardiff, UK) in a non-confocal mode.

2.2. *Time-Gated Detection*

We transformed the CW-STED microscope in a gated CW-STED microscope by simply re-coding fluorescence photons in a time-gated modality (Fig. 1). To implement a real-time gated detection we used a single-photon avalanche diode (SPAD) module developed at Politecnico di Milano (Italy) [27]. The fast-gated SPAD module is a stand-alone single-photon counting instrument capable of turning ON and OFF a silicon SPAD with transition times shorter than 250 ps (20% - 80%). The module is made of two separate blocks: a control unit and a detection head. The control unit contains the electronic circuits needed to synchronize the turn-ON of the SPAD (i.e., the time-gating) with an external trigger source (i.e., the 80 MHz synchronization signal from the Ti:Sapphire laser in our experiments) and to adjust the the gate-width (minimum duration is 2 ns).The detection head contains the SPAD and its dedicated circuitry (a fast pulse generator, the readout electronics and a thermo-electric cooler for temperature-controlled oper-

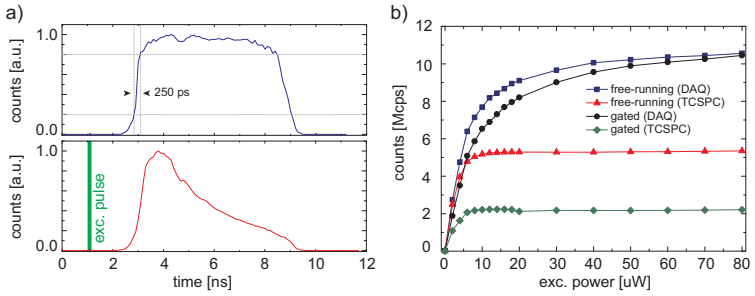

Fig. 2. Fast-gated SPAD module performances. (a, upper panel) Photon counts distribution within a 7 ns gate-ON time window. The light source used was not correlated to the 80 MHz signal which triggered the SPAD. (a, lower panel) Photon counts distribution in case of fluorescence signal. The position of the excitation pulses is marked in green and the gate window is opened after 2 ns. (b) Photon-flux response for linear increasing florescence light focused on the fast-gated SPAD module. Fluorescence has been obtained from a plastic fluorescent slide which has a linear response to the excitation power range used in this experiment (0–80 μW).

ation) and was embedded into the gated CW-STED microscope. The measurement parameters of the fast-gated SPAD module were adjusted using a dedicated software interface developed using LabVIEW environment (National Instruments).

The "photon-OUT" output signal of the control unit is a nuclear instrumentation module (NIM) pulse signal with a duration of 25 ns. Thus before feeding this signal to the data acquisition (DAQ) card (USB-6259-BNC, National Instruments) we converted the NIM compatible signal into a standard transistor-transistor logic (TTL) compatible signal using a custom low-jitter NIM to TTL converter. To fine adjust the time position of the detector's time-gate, with respect to the excitation pulse, we used a picosecond (5 ps random jitter and 10 ps step) delayer (Picosecond Delayer, Micro Photon Devices).

Essential for our experiments is the capability of the module to operate the SPAD also in the free-running mode (i.e., the detector is always ON during the measurement). We used this mode for confocal and conventional CW-STED imaging, for a true comparison between conventional and gated-mode techniques. Furthermore, we used the free-running operation mode to measure the useful photons flux obtained in the case of *a-posteriori* time-gated detection based on a TCSPC card (SPC830, Becker & Hickle). To do this, we fed a replica of the synchronization signal from the laser (as a "stop" signal) and the "photon-OUT" from the fast-gated SPAD module (as a "start" signal) to the TCSPC card (instead of the DAQ card). We also delayed (nanosecond delay box, 7800-7, FAST ComTec Gmbh) the "photon-OUT" signal in order to match it to the linear part of the time-to-analog converter (TAC) of the TCSPC card. For the post-processed time-gated CW-STED measurements, the TCSPC card associates to each photon its arrival time (with respect to the excitation event) and we later sorted only the photons arrived after a specific time-delay T_g.

2.3. Samples Preparation

We measured the maximum and useful photon flux of the detector using a green fluorescent plastic slide (92001, autofluorescent plastic slide, Chroma). The average excited-state lifetime of the fluorescent molecules embedded in the slide is $\tau = 4.4$ ns (single-exponential fitting), thus similar to most of the fluorescent probes used for fluorescence microscopy imaging. We obtained this value using the TCSPC card and the fast-gated detector in the free-running mode.

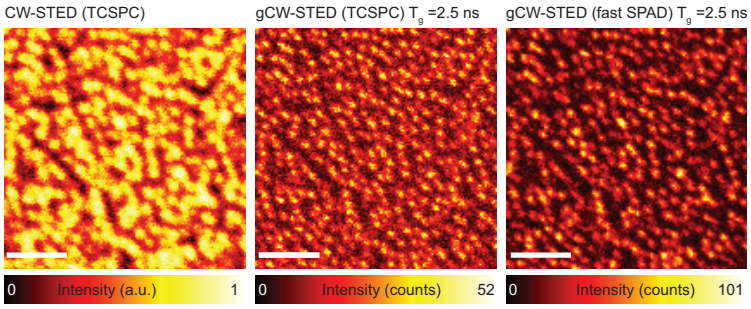

Fig. 3. Comparison of gCW-STED imaging obtained with the fast-gated SPAD module and the TCPSC-based time-gating. P_{exc} = 40 μW, P_{STED} = 100 mW (I^m_{STED} = 50 MWcm^{-2}) and Δ_T = 7 ns. Scale bars 1 μm.

We diluted yellow-green fluorescent calibration nano-beads (40 nm diameter, YellowGreen, Invitrogen) in water 1:1000 (v/v) and we dropped the diluted solution onto a poly-L-lysine (Sigma) coated # 1.5 coverslip. We waited 10 minutes, we washed and dried the coverslip. Finally we mounted the coverslip with a special medium (Mounting Medium, Invitrogen).
The mammalian PtK2 cell line was grown, fixed and immuno-labelled as described previously [30]. Tubulin filaments were stained using a labelling protocol involving a primary antibody (monoclonal mouse anti-α-tubulin antiserum, Sigma Aldrich) and a secondary labelled antibody (Alexa Fluor 488 goat anti-mouse IgG, 1:500, Molecular Probes). Microscopy imaging was performed using an open-bath imaging chamber containing PBS (0.1 M, pH 7.4).

3. Results

An important parameter for the success of the gated STED implementation is the time jitter of the overall time-gated detection system, in terms of (i) jitter on the photon arrival times, (ii) jitter on the aperture of the time window (i.e. jitter on T_g), (iii) time selectivity (i.e. sharpness of rising and falling edges of the time window). High temporal uncertainties can reduce the effective spatial resolution improvement expected by the time-gating. Indeed, such jitter results in the unwanted recording of early-emitted photons, slipping through the gated detection. In our previous work [30], based on a conventional single-photon avalanche diode and a TCSPC card, we had an overall time resolution of $\sim$ 70 ps FWHM (laser pulse-width was $\sim$ 50 ps, TCSPC card resolution was few picoseconds). The dedicated electronics of the fast-gated SPAD module yield a time-jitter lower than 40 ps FWHM on the photon arrival times, $\sim$ 250 ps turn-on-transition (20% – 80%) and less than 20 ps jitter (RMS) on the opening of the time window (Fig. 2(a), upper panel). These values are one order of magnitude smaller than the excited-state lifetime of the fluorophores used in fluorescence microscopy ($\tau < 2 – 4$ ns), thus the effects on the spatial resolution is negligible.
Lower jitter values can be obtained by operating the detector at higher bias voltages, but at the expense of stronger noise (i.e. higher dark count rate - DCR). With the maximum bias voltage (7 V higher than the SPAD breakdown value) the best time resolution was achieved with an acceptable DCR of about 15 kcps (counts per second).
No less important is the maximum repetition rate that the fast-gated SPAD module can sustain, namely the frequency at which the detector can be switched ON and OFF. The prototype used in our measurements works up to 80 MHz, which is fully compatible with the *quasi*-CW excitation beam provided by the home-made 80 MHz super-continuum source and used in these experiments. The 12.5 ns pulse interval gives to the fluorophores enough time to relax to the

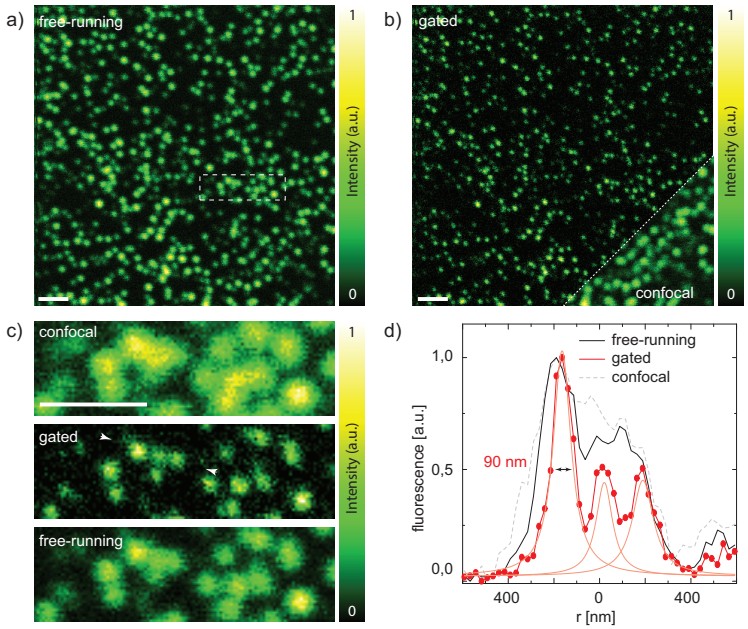

Fig. 4. Gated CW-STED imaging of fluorescent beads using the fast-gated SPAD module. (a) Conventional CW-STED imaging obtained using the fast-gated SPAD in the free-running modality. (b) Gated CW-STED image. The lower-right corner show the confocal recording. (c) Magnified views of the marked areas, renormalized in signal intensity. (d) Intensity profiles along the arrows marked in the gated CW-STED image. P_{exc} = 10 μW, P_{STED} = 50 mW (I^m_{STED} = 25 MWcm^{-2}), T_g = 2 ns and Δ_T = 7 ns. Scale bars 1μm.

ground state before the arrival of the next pulse (which is an important requirement in gated STED microscopy) and optimizes the duty cycle of the fluorescence (which is mandatory for fast imaging) (Fig. 2(a), lower panel). Furthermore, in a gCW-STED microscope, since the STED beam is always active, a longer pulse interval, i.e lower repetition rate, would only produce useless over-illumination of the sample and, in case of direct excitation from the STED beam, an increase of the anti-Stokes fluorescence background. In this context, the possibility to shorten the width of the ON time-window of the fast-gated detector (7 ns in our experiments) allows to reject the anti-Stokes fluorescence photons which can become the majority at times much longer than the excited-state lifetime ($t > 2\tau$).

To demonstrate the ability of the fast-gated detector to increase the useful photon flux in a time-gated experiment, we measured the rate of fluorescent photons stemming from a fluorescent plastic slide with increasing excitation power (Fig. 2(b)). Notably, first we verified that the fluorescent emission flux from the sample behaves linearly along the entire range of excitation beam power used in this experiment (0 – 80 μW). The signal collected using the fast-gated detector in a free-running configuration, i.e., the detector is ON during all the experiment, reaches the saturation rate at 10.5 Mcps, which is equal to the inverse of the dead time of the detector t_d = 95 ns (Fig. 2(b), blue curve). We reached the very same saturation rate when we used a time-gated configuration with Δ_T = 7 ns and time-delay T_g = 1 ns (Fig. 2(b), black curve). This result indicates that the photons reaching the SPAD during its OFF time do not affect the maximum rate of detectable useful photons. Practically, the dynamic range of the time-gated images is not limited by the early photons reaching the SPAD during its OFF time.

The reduction of the useful photon flux in the free-running configuration is evident when the time-gated measurement is obtained *a-posteriori* by means of a TCSPC card (Fig. 2(b)). We repeated the experiment with the fluorescent plastic slide and with the fast-gated SPAD module in the free-running configuration, but this time we fed the output of the detector into the TCSPC card. The longer dead-time of the TCSPC card, with respect to the detector, severely reduces the maximum count rate (5.2 Mcps) of the system (Fig. 2(b), red curve). Furthermore, when the time-gating is obtained *a-posteriori*, since the photons reaching the detector before the time T_g contribute again to the saturation of the system, the maximum count rate for the measurement is further limited (Fig. 2(b), green curve)

The ability of the fast-gated detector to increase the useful photon flux immediately improves the SNR of the gated STED microscopes. To validate this ability, we harmonized the fast-gated detector on a gated CW-STED microscope. We first tested the system to visualize yellow-green fluorescent calibration nano-beads. According to Fig. 2(b), the benefits of the fast-gated SPAD increase for high photon emission flux. To highlight these benefits, we used an excitation power ($P_{exc} = 40\ \mu W$) able to generate a photon emission flux (from the fluorescent beads) which saturates the TCSPC card. Figure 3 shows a side-by-side comparison between gCW-STED images obtained using the TCSPC card (the fast-gated SPAD run in the free running mode) and the fast-gated SPAD. The saturation of the TCSPC-based imaging system is evident at null time-gating (T_g = 0 ns, CW-STED modality): Almost every pixel value is toward the right side of the histogram. Furthermore, the SNR reduces (peak SNR $\sim$ 7) for longer time-delay (T_g = 2.5 ns). In contrast, the gCW-STED image obtained with the fast-gated SPAD and in the very same conditions (power of the excitation beam, pixel-dwell time, time-delay T_g and gate-width Δ_T) shows higher SNR (peak SNR $\sim$ 10).

The combination of low time-jitter, high repetition-rate, high effective count-rate and intrinsic time-selectivity makes the fast-gated SPAD module the ideal detector to implement a gated STED microscope, with the additional benefit of a significant simplification of the overall system architecture (neither post processing nor other external gating systems are needed). In particular, the SNR improvement allows to fully explore the potential of gCW-STED microscopy, namely to work at low STED beam power, and to reach exquisite resolution by using long time-delays. We therefore made STED imaging at relatively low STED beam power (P_{STED} = 50 mW, I^m_{STED} = 25 MWcm^{-2}). At this power range almost no resolution improvement is expected from the conventional CW-STED microscope (no time-gating). Figure 4 shows imaging of yellow-green fluorescent calibration beads. The comparison between the conventional CW-STED image (Fig. 4(a)), i.e., the detector works in the free-running configuration, and the confocal image (Fig. 4(b), lower right corner) shows a weak resolution improvement. The resolution of the STED image significantly improves in the time-gated configuration (Fig. 4(b)). The different magnifications of a convoluted region of the sample (Fig. 4(c)) and the intensity lines profiles of closely spaced fluorescent beads (Fig. 4(d)) underline the spatial resolution strengths for the different imaging modalities.

Similar results and observations where obtained when imaging immunolabelled micrtotubule network of a PtK2 cell (Fig. 5). With respect to the confocal image the gCW-STED image based on the fast-gated SPAD reveals the convoluted structures of the microtubule network.

Finally, it is important to note that in comparison with the TCSPC-based implementation the fast-gated SPAD module implementation does not need to store the photon-arrival times, thus the frame rate of the system is not hindered by the data buffering operation.

4. Conclusions

The costs, the complexity and the high light-intensity demand were strong limitations for a wide spread use of super-resolved STED microscopy. Nowadays, these constraints have effec-

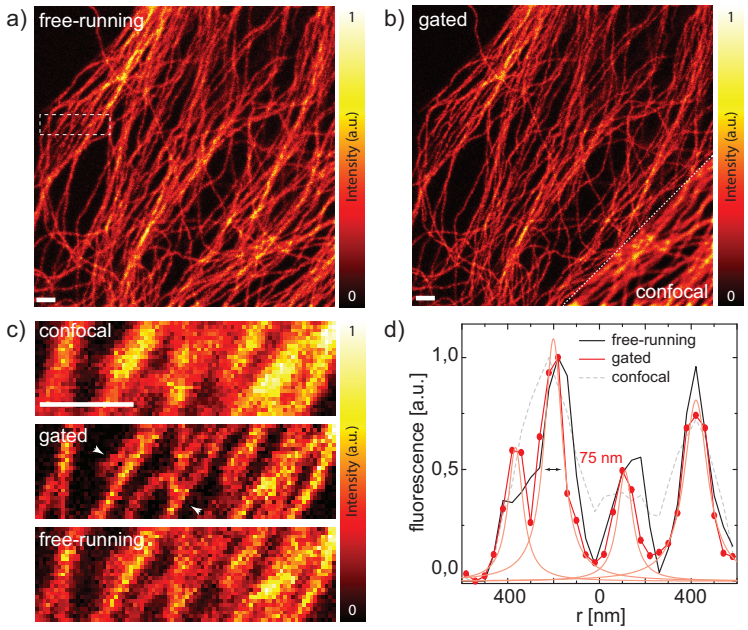

Fig. 5. Gated CW-STED imaging of a microtubuline network using the fast-gated SPAD module. (a) Conventional CW-STED imaging obtained using the fast-gated SPAD in the free-running modality. (b) Gated CW-STED image. The lower-right corner show the confocal recording. (c) Magnified views of the marked areas, renormalized in signal intensity. (d) Intensity profiles along the arrows marked in the gated CW-STED image. $P_{exc} = 10\ \mu$W, $P_{STED} = 50$ mW ($I^m_{STED} = 25$ MWcm^{-2}), $T_g = 2$ ns and $\Delta_T = 7$ ns. Scale bars 1μm.

tively relaxed and applications and studies using STED microscopy are growing exponentially. An important contribution towards this success has been given by the introduction of the time-gated detection in the STED microscopy architecture. By collecting fluorescent photons after a time-delay from the fluorophores' excitation events, the STED beam intensity needed to reach a certain spatial resolution substantially reduces. Furthermore, this lower intensity opens the possibility to realize new STED microscopy implementations based on nanosecond pulsed or CW laser source, which reduce complexity and costs.

However, the benefits of the time-gated detection for STED microscopy come along with a reduction of the SNR and SBR of the images. Here, we showed that the fast-gated SPAD can mitigate these reductions. The fast gated SPAD increases the effective photons collections efficiency of a time-gated STED microscope, without increasing the complexity of the system or reducing its versatility.

Acknowledgements

The authors are grateful to Alessandro Barcellona (Istituto Italiano di Tecnologia) for technical assistance and Marta d'Amora (Istituto Italiano di Tecnologia) for sample preparation. This work was supported in part by PRIN N. 2008S22MJC 005 [A.D. and G.V.] grant.